Fabrication and characterization of *p*-type silicon field-emitter arrays for lithography

T. F. Teepen, A. H. V. van Veen, H. van't Spijker, S. W. H. K. Steenbrink, A. van Zuuk, C. Th. H. Heerkens, and M. J. Wieland
Mapper Lithography, Lorentzweg 1, 2628 CJ Delft, The Netherlands

N. J. van Druten[a] and P. Kruit[b]
Delft University of Technology, Lorentzweg 1, 2628 CJ Delft, The Netherlands

(Received 26 July 2004; accepted 27 December 2004; published 17 February 2005)

p-doped silicon field emitters were studied experimentally to assess their usefulness in multibeam electron lithography. Both individual emitters and emitter arrays were fabricated from single crystal Si wafers with several doping levels. Current-voltage curves were measured for different temperatures and illumination conditions. The typical plateaus in the *I-V* curves and the sensitivity to light known from the literature were reproduced. Stability measurements showed a very stable total emission current even while the angular emission distribution fluctuated strongly, giving unstable currents in apertured beams. Measured light response times varied between 34 ns and 20 μs, depending on experimental conditions. It was found that in the plateau of the *I-V* curve, the energy of the electrons shifts over up to 100 eV when changing the extraction voltage over a few kilovolts. In operation, when the current is stable, the energy shift is rather unstable. The experimental results are discussed within a model of the emission process involving an induced *p-n* junction inside the tip. The conclusion is that *p*-doped silicon field emitters are not particularly useful for applications in electron beam lithography. © *2005 American Vacuum Society.*
[DOI: 10.1116/1.1861045]

I. INTRODUCTION

Silicon field emitters have been considered as electron sources for many different applications: flat screen displays, vacuum microelectronic devices, electron microscopes, microwave tubes, lithography apparatus, even for photocathodes.[1] *p*-type silicon emitters have drawn special attention because under certain operating conditions, the emission current can be extremely stable.[2] In addition, the emission can be switched on and off by illumination with visible light.[3,4] We became interested in the use of *p*-doped silicon emitters for multi beam electron lithography. Electron beam lithography is a relatively old subject: Electron beam pattern generators have been in use for several decades, both in academic labs for writing nanostructures and in industry for writing masks and prototype electronic circuits. The use for direct patterning of silicon is limited because of the throughput problem: Although the resolution approaches 10 nm, it takes many hours to write one full wafer, even with 50 nm patterns. Yet there are new efforts to increase the throughput as the industry moves toward 45 nm design rules. The move to systems with a large number of beams in parallel is almost inescapable. Depending on the writing strategy this number may vary from several hundreds to even a million beams in parallel.[5] If an array of light sensitive field emitters could be produced with the right properties, this would be the ideal source for such a system. The requirements for lithography are fairly stringent. For a typical system with multiple Gaussian beams, each beam must focus a few nanoamperes into a spot of a few tens of nanometers. This results in strict demands both on source brightness and on energy spread. The current must be stable to within a few percent and all beams must contain the same current to within a few percent. Since one pixel (design rule or critical dimension squared) in the written pattern contains only a few thousand electrons and the edge position must be defined to within a fraction of that pixel, the beam must be switched off or on within the order of nanoseconds. In such a short time, the beam delivers only a few hundred electrons. Published experimental results by Schroder *et al.*[6] were very promising: large arrays of emitters with homogeneous and stable emission, sensitive to light with high quantum yields and, when cooled, low dark current. The authors had examined their usefulness for photocathode applications. For our application we also needed to know properties such as time-response, virtual source sizes, emission angles, energy spread of the beams, stability of apertured beams, stability of beam direction, and cross talk between emitters. A good model of these "photo field emitters" or "semiconductor field-emission cathodes" or "field emission photo cathodes (FEP)" would have helped to make predictions of those properties. However, although the literature on the subject started in 1952 (Ref. 7) and several groups have suggested models,[4,8–11] we could not find a clear, unambiguous, quantitative model. We performed many experiments on individual emitters and small arrays of emitters, the results of which we describe in the present paper. In order to have a theoretical context for discussing the experimental results, the next section will first describe our

[a]Present address: Van der Waals-Zeeman Instituut, Universiteit van Amsterdam Valckenierstraat 65-67, Amsterdam, The Netherlands.
[b]Electronic mail: P.Kruit@tnw.tudelft.nl

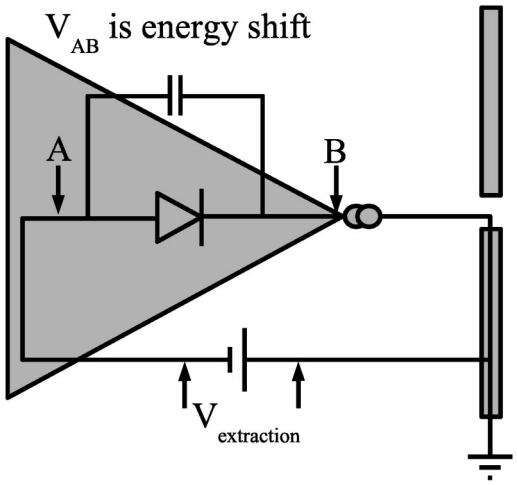

FIG. 1. Electrical circuit that models the *p*-type Si field emitter tip.

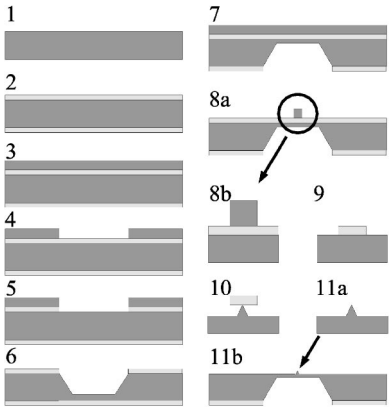

FIG. 2. Schematic overview of the process steps involved in making *p*-type silicon emitters.

presently preferred model for field emission from *p*-type semiconductors, based both on models in the literature, especially from Arthur,[8] Schroder *et al.*,[6] and Hirano *et al.*[12] and on our own observations.

II. EMISSION MODEL

Field emission is usually modeled using the Fowler–Nordheim (F–N) theory.[13] The theory gives the emission current density as a function of electric field strength on the surface, the work function, and the electron density in the material. The electric field strength on the tip depends not only on the applied extraction voltage, but also on the tip height, tip radius, and shape, through the "field enhancement factor" (β). We assume that the F–N theory is basically still valid, but for *p*-type semiconductors it is more complicated to find the electron density and the field on the surface. An external field on a semiconductor causes band bending and field penetration. At the extreme fields necessary for field emission the band bending is sufficient to create a *n*-type layer at the apex. The electrons in the *n*-type apex are also necessary to have a smaller field inside the tip than outside the tip. With the *n*-type apex on the *p*-type material, a *p*-*n* junction is created inside the tip, with its associated depletion layer. When a current is drawn from the tip, the junction is in reverse bias, with a junction voltage that is determined by the current through the junction. The junction voltage reduces the field at the apex, not just because the extraction voltage is effectively lower, but much more because of a lower field-enhancement factor. This can be understood by realizing that the enhancement is totally gone when the voltage over the tip is equal to the average cathode-anode field times the height of the tip. The model is summarized by the electric circuit of Fig. 1. The circuit consists of a current source at the tip of the emitter, in series with a *p*-*n* junction or diode in reverse bias with a capacitance in parallel. Between the field emission photo cathode (FEP) and the extractor (drawn here as an extractor aperture), an extraction potential is applied ($V_{extractor}$). With this model four different regimes for the applied extraction potential can be distinguished. In the first regime $V_{extractor}$ is small such that the emission current is smaller than the diode dark current. In this regime the current is therefore not limited by the diode but by the transparency of the surface-vacuum barrier. With increasing $V_{extractor}$ the surface-vacuum barrier becomes more transparent and the emission current increases. Since the transparency of the surface vacuum barrier determines the emission current, all processes that change the transparency of the surface vacuum barrier (for instance: gas atoms moving on and off the tip) influence the emission current. At a certain $V_{extractor}$ the diode limits the emission current at a level equal to the diode dark current. In this second regime the current is almost constant with increasing $V_{extractor}$ and is invariant to changes of the transparency of the surface-vacuum barrier. However, a small change in current gives a large change of the junction voltage. This regime is called the plateau region. In the third region $V_{extractor}$ is such that the potential over the diode exceeds the breakdown voltage of the diode, resulting in a large supply of electrons to the emitter tip. The current will increase rapidly until the transparency of the surface-vacuum barrier is again the current-limiting factor (region 4). The dark current and breakdown voltage of the diode are related to the doping level of the *p*-type Si. The dark current of the diode can also be changed by the amount of light incident on the FEP. With the extraction potential set such that the emitter is operated in the plateau regime the emission current can therefore be modulated by the amount of light incident on the FEP; i.e., modulating the diode dark current. The capacitance in Fig. 1 is a combination of the junction capacitance and the capacitance between the apex and the extractor electrode. It results in a small delay in the feedback loop and limits the light response time. Since the capacitance is small, it can only be detected for small currents.

III. FABRICATION

The *p*-type silicon field emitter array samples are fabricated at the clean-room facility DIMES of Delft University of Technology. The fabrication is done in a series of steps, see Fig. 2. A single side polished (1) *p*-type Si wafer with the

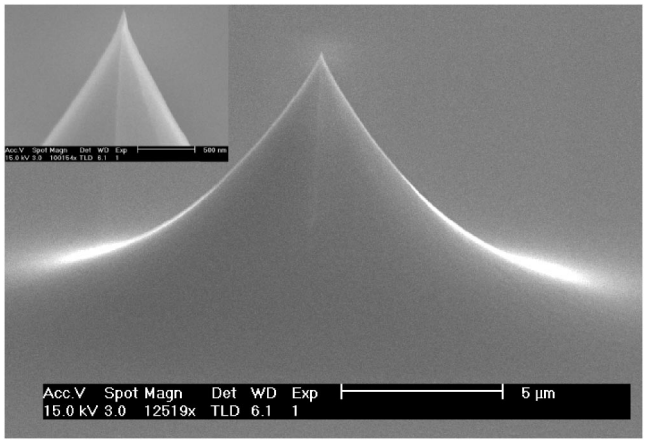

FIG. 3. Typical *p*-type silicon single emitter fabricated at DIMES with in inset a zoom-in image of the emitter tip.

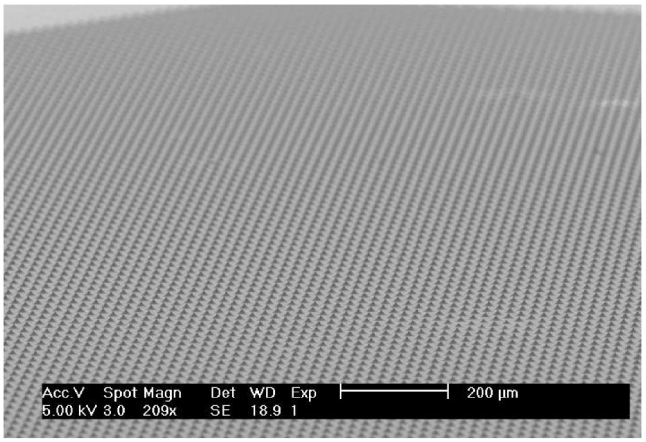

FIG. 4. Large array of about 4000 emitters fabricated at DIMES.

desired resistivity is used. A layer of Si_xN_y of 100 nm or more is deposited on both sides by low pressure chemical vapor deposition (2). Next the backside is spin coated with resist and exposed with near ultra violet (NUV) (3) and (4). After developing the backside, the pattern in resist is transferred into the nitride layer (5). Then the wafer is etched with KOH until a membrane of about 40 μm is left (6). The membrane is essential to enable backside illumination of the sample. It must be sufficiently thin for either the light or the photoelectrons to reach the depletion layer in the tip. For the fabrication of the emitters the desired array of circles is printed in resist (7) with NUV (8). Again this pattern is transferred into the nitride layer using a CHF_3/O_2 plasma (9). After the pattern transfer, a short HF dip is performed to remove the thin oxide layer present on the bare silicon. Thereafter the wafer is etched isotropic with HNA-etch (HF + nitric acid + acetic acid) to create an array of emitters in Si (10). After the tips are formed the wafer is thoroughly cleaned in a solution of 5 parts H_2O, 2 parts H_2O_2, and 1 part NH_4. The tip radii of the emitters is reduced by thermal oxidation and HF dipping for oxide removal until the emitters on the membrane have tip radii of 10–20 nm (11). Figure 3 shows a typical image of an emitter after fabrication and oxidation. In Fig. 4 the largest array fabricated is shown, this array consists of 4000 emitters.

IV. EXPERIMENTAL SETUPS

All experimental setups consist of a vacuum chamber with an operating pressure of 10^{-7}–10^{-8} mbar. The samples are mounted in a custom made polished sample holder that is connected to a voltage source that can change the voltage from −10 to 0 kV. In Fig. 5 a schematic overview of the three setups used is given. At a distance of about 0.6 mm from the sample either a YAG screen (setup 1 and 3) or an extraction aperture of about 500 μm (setup 2) is placed. The YAG screen or the aperture are both mounted in a polished holder and connected to a voltage source that can change the potential from 0 to +10 kV. In setup 3 the YAG-sample distance can be changed. In setup 2 behind the extraction aperture at a distance of 10 mm, a plate with a 5 mm hole at 0 V is positioned with a metal cylinder for electrical shielding of the electron beam from the contacting wires. The sample is thermally connected to an ethanol-cooling unit that can control the temperature of the sample between room temperature and −90 °C (setup 1) and −20 °C (setup 2). The emission current can be measured directly with a current meter connected to the YAG screen and indirectly by means of a photomultiplier (pm) that detects the light from the YAG screen. Setup 2 has the possibility of inserting a retarding grid in the electron beam consisting of three parallel grids at a distance of about 2 mm apart, with grid sizes of 60 μm; 30 μm and 1 mm, respectively. The grid is used for measuring the energy of the emitted electrons. Setup 3 has two microscope objectives inside the vacuum chamber. These objectives are used to focus the laser on the FEP with a spot

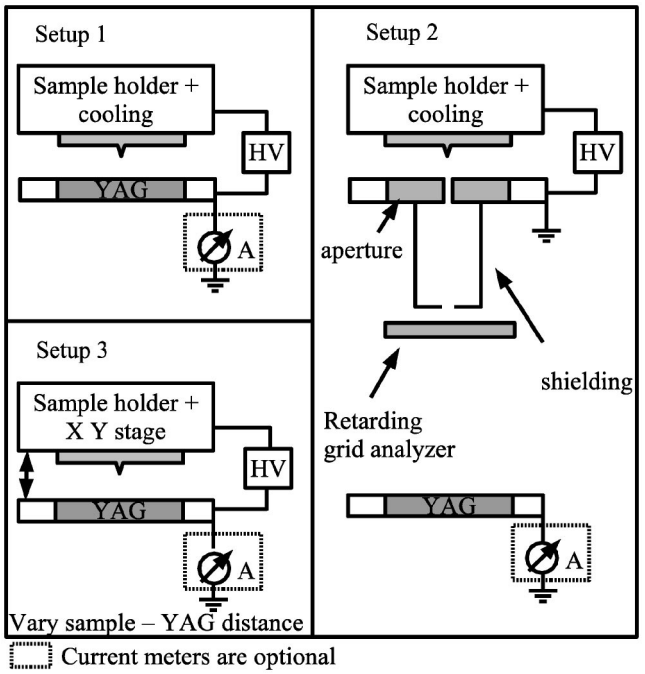

FIG. 5. Schematic overview of the three setups used for the measurements.

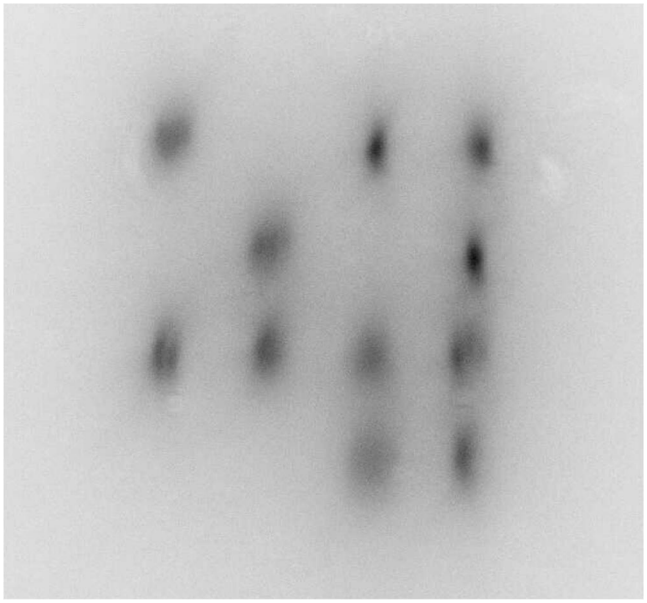

FIG. 6. Typical CCD image of the emission current from a 4×4 array on a YAG screen

size of about 6 μm. The second objective is for detecting the e-beam spots on the YAG screen. The FEP sample holder can be moved with a piezostage with an accuracy of better than 10 nm. The whole experiment is immersed in a magnetic field of up to 0.5 T that can focus the beam from the emitter to the YAG screen. For illumination of the emitters a 658 nm, 25 mW laser diode is used that illuminates the emitters from the backside of the sample. The switching time of this diode is 50 ns. For the ultra fast light response measurements a fast 658 nm, a 10 ns diode laser is used.

V. EXPERIMENTAL RESULTS

Most experiments are performed on samples with a single emitter tip. Only for statistical information on the yield of the emitters a few measurements were made on multiple emitter samples. From these measurements it is clear that the yield is over 50% without optimizing the fabrication method. In Fig. 6 the typical emission pattern on a YAG screen from a 4×4 emitter array in setup 1 is shown. The picture is taken with a charge-coupled device (CCD) camera. In this figure one can see that about 70% of the emitters are working.

A. *I-V* characteristics

Several authors have published emission current-extraction voltage (*I-V*) measurements on arrays of *p*-type Si emitters, often presented in the form of Fowler–Nordheim plots. In particular, the work of Thomas, and Schroder *et al.*,[6] Thomas *et al.*,[14] and Thomas and Nathanson[15] Nathanson,[3] demonstrates clearly, as a function of temperature and light intensity, the occurrance of a plateau region, where the emission current is independent of extraction voltage. No measurements on microscopic individual silicon tips have been performed to date. Our *I-V* measurements on single emitters consist of changing either the sample or the aperture/YAG

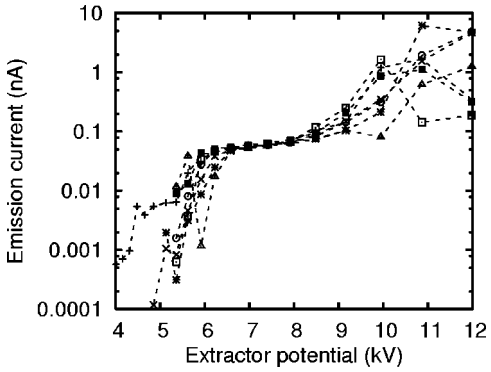

FIG. 7. Dark current *I-V* characteristics of a highly *p*-doped single emitter at room temperature.

potential and measuring the emission current. In Fig. 7 a typical set of *I-V* measurements is shown. The measurement is performed on a 0.01 Ω cm sample at room temperature with no light incident on the FEP (dark current). The unique feature of these measurements is that the different curves are measured right after each other, as fast as possible, trying to keep the apex condition of the tip unchanged during the measurement of a full curve. Each curve takes about 20 s, which is determined by the time needed to stabilize the extraction potential. Figure 7 now clearly shows the origin of the stability of the current in the plateau region. The instability of the current in region 1 and 4 (see discussion of emission model) is clearly visible: For a given extraction potential, the current may fluctuate over more than an order of magnitude. Changes in work function or shape of the apex due to residual gas atoms are manifested as shifts in the *I-V* curves with respect to the extractor potential. Only in the plateau region, the emission current is determined by the amount of electrons generated in the depletion region of the emitter (diode dark current). The diode dark current is dependent on the temperature. In Fig. 8 dark current *I-V* measurements on a 20 Ω cm sample for different temperatures are shown. The lowest curve in Fig. 8 is the current measurement limit of setup 1 which is calculated from the sensitivity of the photomultiplier for the light from the YAG screen and corrected for the energy of the electrons. The figure shows clearly that

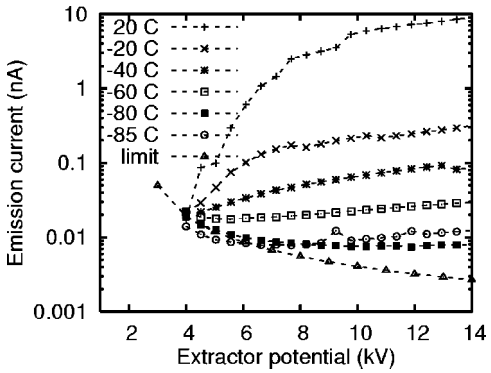

FIG. 8. Dark current *I-V* characteristics of a 20 Ω^* cm single emitter at different temperatures.

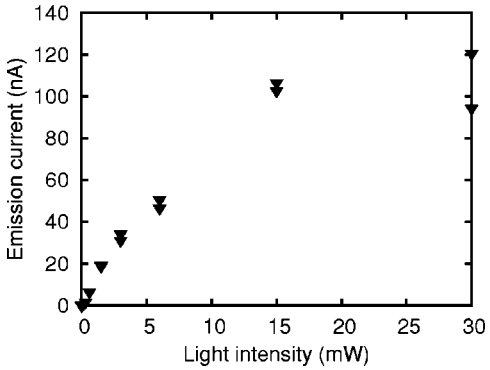

FIG. 9. Emission current at 14 kV, −85 °C for different light powers incident on the FEP.

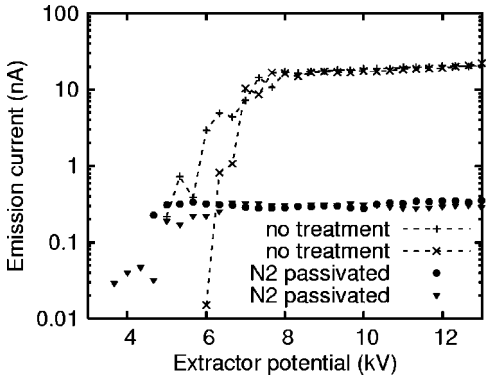

FIG. 11. Dark current *I-V* characteristics at room temperature of different samples with and without a N_2 annealing step.

with a change in temperature from 20 °C to −85 °C a change in emission current of three decades (10 pA–10 nA at 14 kV) is realized. The different plateaus in the plot are parallel, which indicates that the dark current of the diode is indeed the limiting factor and that the surface vacuum barrier is not of any influence on the *I-V* characteristic in this region. The amount of electrons generated in the depletion region at a certain temperature can also be changed by exciting electrons with light. In Fig. 9 the emission current change with the change of the amount of light power incident on the FEP at −85 °C and 14 kV is shown. The data is extracted from *I-V* characteristics at the different light intensities. At low light intensities (< 3 mW) the current increases linearly with the light power. For larger light intensities the current starts to saturate. Since only electron hole pairs generated within the depletion region are separated resulting in an emission current, the width of the depletion region, which is influenced by the doping concentration, determines the dark current. In Fig. 10 dark current *I-V* characteristics of samples with different doping levels at room temperature are shown. All *I-V* characteristics in Fig. 10 show a plateau starting at about 6 kV. This is determined by the physical shapes of the emitters, which are similar since the fabrication method is the same for all emitters (similar β and thus similar field at the emitter tip). The end and the height of the plateau are determined by the size of the depletion region and thus change for different doping levels. For high doping levels (low resistivity), the depletion region is smaller and therefore the internal diode breakdown field is reached sooner and the dark current is smaller. This is best visible in the lowest plot in Fig. 10, where a small plateau is visible. The size of the other plateaus is unknown since it is outside the scope of the setup (10 kV max for setup 1 and 20 kV max for setups 2 and 3), but it is clearly larger which is expected from the doping level. Figure 10 shows the increase in dark current with decreasing doping level (larger resistivity). The dark current is partly generated at surface states;[6,16] this effect is well known for *p-n* junctions in metal-oxide-semiconductor devices. The surface states exist mainly on the Si SiO_2 interface where there is a structural mismatch between the S lattice and the slightly larger SiO_2 lattice. The amount of surface states can be reduced by passivation of the Si–SiO_2 interface.[17,18] There are many different methods to passivate this interface. In Fig. 11 the result of N_2O passivation on the dark current at room temperature is shown. For this plot, two samples are shown which have been measured both before and after passivation.

B. Current stability

Although current from *p*-type Si emitters is often reported to be "stable" in the plateau region, quantitative stability measurements on individual tips are rare.[2] In Fig. 12, a full

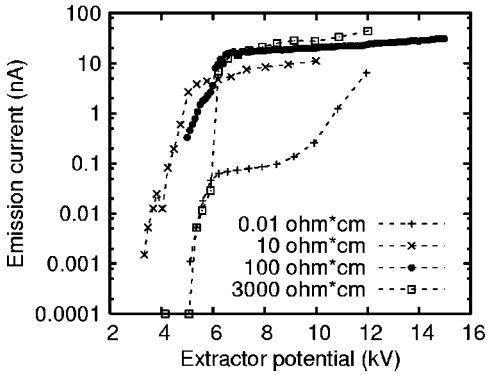

FIG. 10. Dark current *I-V* characteristics of samples with different doping levels at room temperature.

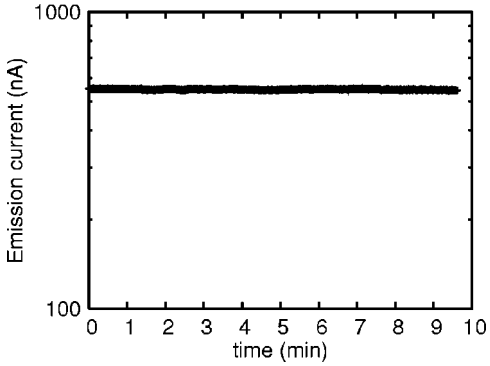

FIG. 12. Current stability at plateau region with 30 mW, 658 nm laser illumination is smaller than 1% 3σ.

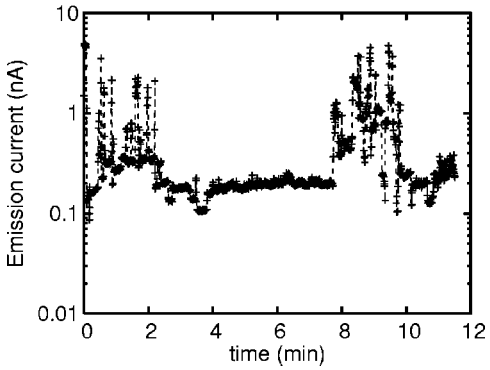

FIG. 13. Current stability not on the plateau, the current fluctuates over about two orders of magnitude.

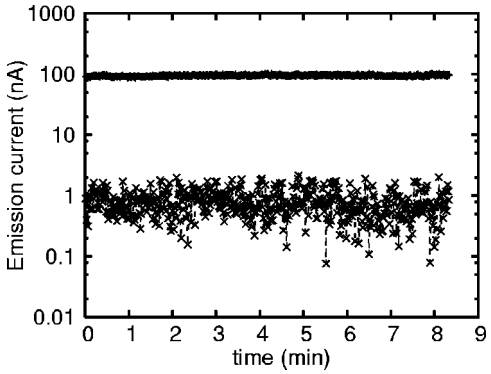

FIG. 15. Current stability at plateau region without (top) and with (bottom) an aperture (1% of total area). The stability is 3% and 50% 3σ, respectively.

laser current stability measurement at room temperature is shown over a time period of 10 min. The stability is better than 1% 3σ, which is extremely stable in contrast to the stability of the emission current in region 1 as shown in Fig. 13. The current in this region is determined by the surface vacuum barrier and therefore changes with every atom moving on and off the emitter tip. One atom change, for instance, moving on the tip, changes the work function dramatically; the surface vacuum barrier becomes more transparent and the emission current increases. The current in Fig. 13 shows this behavior clearly; here the emission current changes almost two orders of magnitude during the stability measurement. In Fig. 12 the total emission current is very stable but still residual gas atoms do move on and off the emitter tip, changing work function and shape. The reason that the total emission current does not change, according to our model, is that the field at the apex is adjusted by the intrinsic feedback mechanism. However, this feedback mechanism does not guarantee that the emission will also be in the same direction

In Fig. 14 we show angular current density patterns from the same tip at different times. It is clear that the patterns change, while the total emission current is stable. The lack of detail in the plots indicates that the tips are very sharp. Occasionally, we see the typical structures that are also seen from carbon nanotubes,[19] with two or four lobes that are interpreted as fully coherent emission through double or quadruple emission sites. In Fig. 15 two current stability measurements are shown at room temperature with light incident on the FEP. The top plot is of the current stability of the total emission current; the bottom plot shows the current during the same period measured through a fixed aperture of about 1% of the total emission spot on the YAG screen. The bottom plot is clearly less stable than the top plot. This shows that the residual gas atoms result in an angular current density change, which results in an unstable emission current in a small fixed area of the total emission area on the YAG screen. The stability is 3% and 50% 3σ for the top and bottom plot, respectively. The current stability plots described

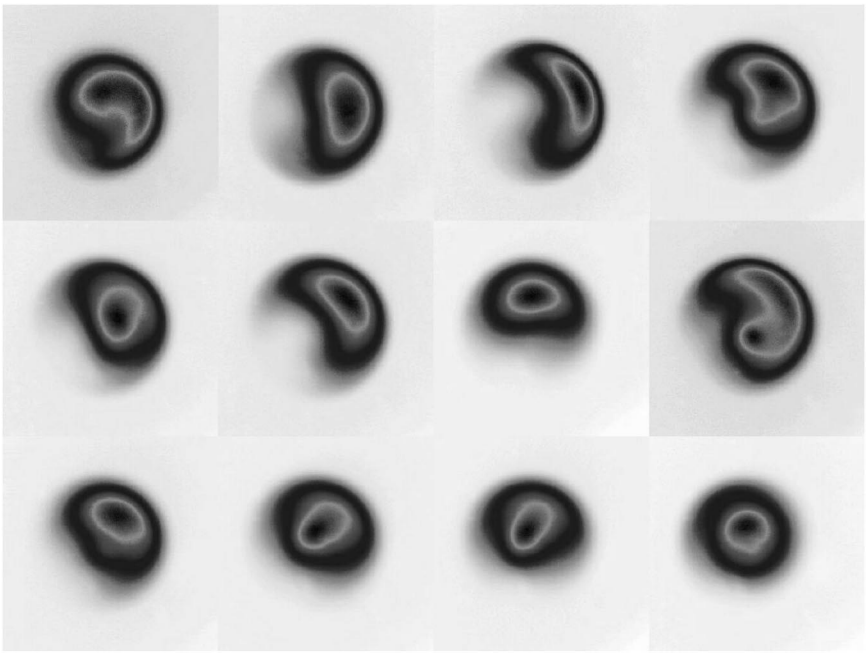

FIG. 14. CCD images of an emission pattern of a single emitter at different times.

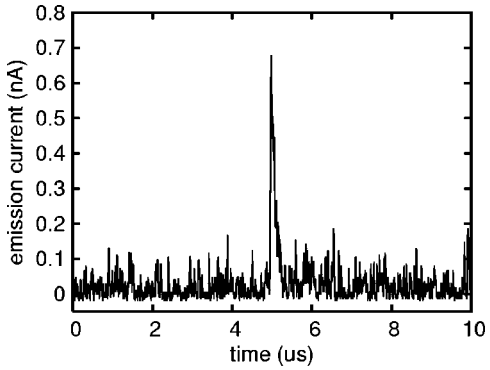

FIG. 16. Current peak during dark current stability measurement. The surface below the peak amounts to about 600 electrons.

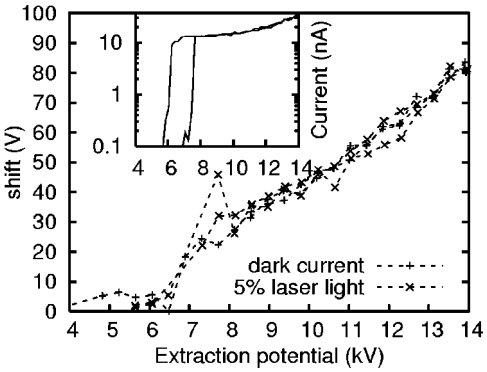

FIG. 17. Energy shift change with changing extractor potential at room temperature.

above are long-term (up to 10 min) stability measurements. In Fig. 16 a short-term dark current stability in the plateau region is shown. The current is quite stable but regularly a peak in the current is observed. The peak can only be made visible at very low emission currents. The data in the figure is recorded at $-20\,^{\circ}\mathrm{C}$. The number of electrons associated with this peak is about 600. This is the reason why the peak can only be observed at small currents; otherwise the measurement system cannot distinguish it from the noise. A large portion of the variation measured in the background in Fig. 16 is poison noise. We interpret this measurement as the proof of a feedback mechanism: It takes a certain charge and thus time for the reverse diode in the tip to adjust its voltage drop and adjust the field at the apex.

C. Energy shift

Measurements of the energy of the emitted electrons on large single *p*-Si emitter tips on the end of a wire[8,10,20,21] show large potential drops over the emitter: up to 2 kV at an extraction potential of 6 kV. The potential drop depended on extraction potential and illumination level. No measurements on the potential drop or energy shift are known on emitters of micrometer size.

The energy shift during a standard *I-V* measurement is recorded in our experiments by measuring the energy spread at each point of the *I-V* curve. The difference between the center of the energy spread and the sample potential is the energy shift. In Fig. 17, a typical shift measurement at room temperature is shown. The energy of the emitted electrons clearly changes with the applied field. In region 1 (<6 kV) the shift is constant, changing into a shift that is almost linear with the change in extraction field. The inset in Fig. 17 shows the *I-V* characteristic of this tip while illuminated with light. It is interesting to see that the plateau region starts at about 6 kV: the same point at which the energy shift starts to increase. Our interpretation is that at this point the diode starts to limit the current. The shift measurements in Fig. 17 are time averaged. In Fig. 18, the shift (for a different tip than of Fig. 17) is plotted as a function of emission current. The individual measurement points, from a retarding field energy scan, were made as fast as possible, because the en-

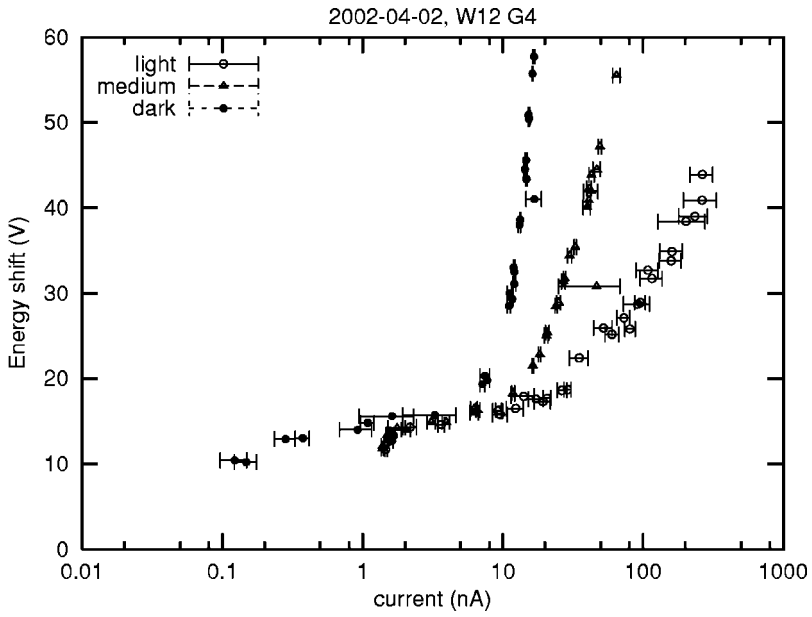

FIG. 18. Energy shift plotted as a function of emission current for three different light intensities. Notice the typical behavior of a light illuminated diode.

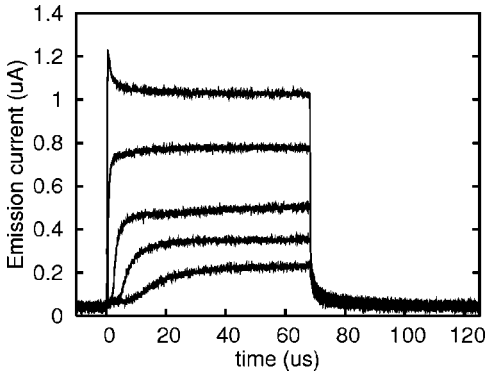

FIG. 19. Light response of the FEP on different light intensities at room temperature.

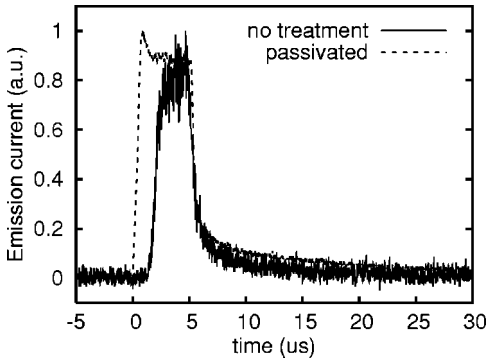

FIG. 20. Light response of the FEP at room temperature before and after at constant light intensity with scaled emission current.

ergy shift turned out to be very unstable. The error bars in Fig. 18 give the variation in total emission current for each measurement point. Part of the emission current axis could be filled by measurements at one extraction voltage, because the shift jumped over a range of typically 10 to 25 V. In the dark current measurement, the shift jumps are large, but the current jumps are small. With light illumination, the energy jumps are a bit smaller, but the current jumps larger. Given an extraction voltage, the shift decreases slowly with increasing light intensity. The shift offset of about 10 V is unexplained, but the rest of the curves show the typical behavior of a light illuminated diode.

D. Light response

There is not much known about the transient response of the emission of a photo field emitter to a light pulse. There is some work done on the response on a light pulse of a field emission array,[4] where typical response times varied from the millisecond range to the submicrosecond range depending on extraction potential, illumination level, temperature, and thickness of the sample.

The switching speed of one of our tips is shown in Fig. 19. The light intensity decreases with the maximum emission current of the different plots. The measurements are performed at room temperature. At $t=0$ μs the laser is switched on and at $t=70$ μs it is switched off again. Figure 19 clearly shows that the switch-on speed of the FEP changes with the maximum emission current; large current results in fast switching. The switch-off time is almost constant. The fastest switch on and off time measured is 34 and 130 ns, respectively. Figure 11 shows the impact of passivation on the dark current of the FEP. In Fig. 20 the result of H2 passivation on light response is shown. At $t=0$ μs the laser is turned on and at $t=5$ μs it is turned off again. The amount of light incident on the FEP and the extraction potential is kept constant in both measurements but the emission current changed a lot after passivation; for clarity, the emission current is scaled to compare the two light response curves. We interpret this as a change in the diode capacitance through the passivation of surface defects. The measurements performed above used a relatively large laser spot of about 1 mm on the backside of the FEP to ensure an easy alignment of the laser on the FEP. In order to measure the light sensitive area, the spot size of the laser is about 6 μm. The FEP is scanned with a stage perpendicular to the laser beam and simultaneously the emission current is detected. The measurements are performed at different light intensities and at room temperature with both a 2000 and 85 Ω cm FEP. In Fig. 21 the light sensitive area of the two samples is shown. All data is normalized for comparison and the top three data sets are shifted for clarity. From Fig. 21 it is clear that increasing the light power has an effect on the light sensitive area. For the 2000 Ω cm sample the full width at half maximum changes with light power from 75 to 51 μm for 66 and 0.66 μW laser incident on the FEP. The 85 Ω cm sample clearly has a smaller detection area which is about 17 μm with 22 μW laser light incident on the FEP. For larger light intensities and smaller resistivity (higher p doped) the light sensitive area decreases. The diameter of the base of the emitter is about 10 μm. In Fig. 9 the emission current change with respect to the light power is shown. Since the light spot of the laser used for this measurement was larger than the detection area of the emitter it is not possible to calculate the quantum efficiency of the FEP from this figure. In Fig. 22 the quantum efficiency of a 2000 Ω cm FEP at room temperature is shown. The laser light used was focused to a spot of 6 μm and scanned over the backside of the FEP; the maximum current of the scan is

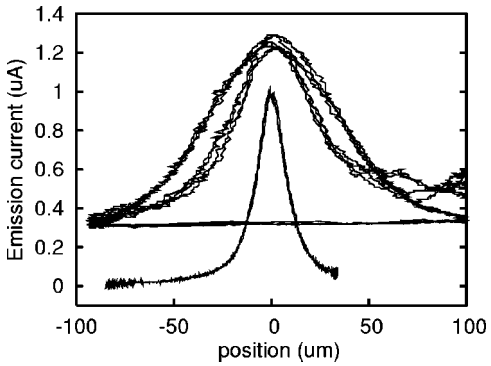

FIG. 21. Light sensitive area for two different FEP samples. Top plot is 2000 Ω^* cm at 66, 0.66, and 0μ W laser power respectively and bottom plot is a 85 Ω^* cm at 22μ W.

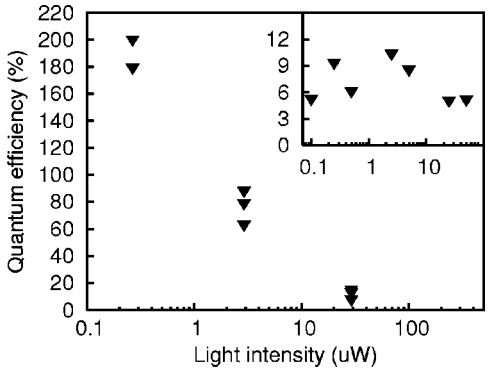

FIG. 22. Quantum efficiency of a 2000 Ω^* cm FEP. The inset shows the quantum efficiency of a 85 Ω^* cm FEP, both at room temperature.

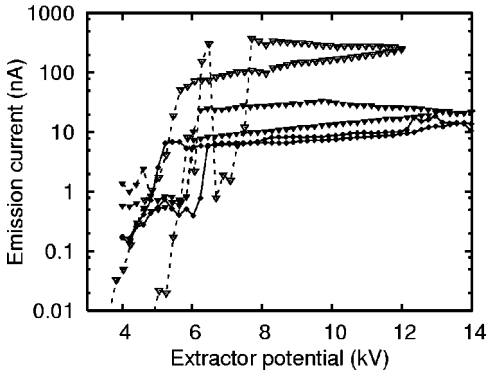

FIG. 24. Dark current *I-V* characteristics with onset of a FEP where the first *I-V* curve has larger emission current in the plateau region which decreases until it is constant.

used for the calculation of the quantum efficiency. All losses for glass, filters, and mirrors are taken into account for the calculation of the quantum efficiency. In Fig. 22 it is clear that the quantum efficiency drops dramatically from about 200% to less than 20% with increasing light intensity. This is consistent with the data shown in Fig. 9 where the emission current remains constant with increasing light power above 15 mW. The inset of Fig. 22 shows the measurements of the quantum efficiency of a 85 Ω cm sample. Here the quantum efficiency is constant (within a few percent) over about the same intensity range, which is also consistent with the data shown in Fig. 9. The quantum efficiency for high resistivity samples is clearly larger than that of low resistivity samples.

E. Onset

Usually the measurements on the FEP showed curious behavior at the first few *I-V* characteristics after fabrication. The first *I-V* characteristic differs considerably from the *I-V* characteristics measured later on. This onset effect is shown in Figs. 23 and 24 showing two different kind of onset behavior encountered. Both plots show dark current *I-V* characteristics at room temperature of new FEP samples and without any treatment except for inserting in vacuum before starting the *I-V* measurement. In Fig. 23 it is shown that the FEP does not yet work until past the field necessary in subsequent measurements. The second type of onset is shown in Fig. 24 where the emission current in the plateau region in the first *I-V* curve is very large and decreases until it is constant. This decreasing of the current is clearly an emission current induced phenomenon, since stopping the measurement after one *I-V* curve and starting again later on results in the same plot as shown here where the *I-V* measurements are recorded right after each other. It was investigated if the onset is a surface induced effect by oxidizing and HF dipping the FEP several times between measurements. The onset effect did return but no correlation between the amount of oxide growth and removal steps was found. We do not understand the onset phenomena.

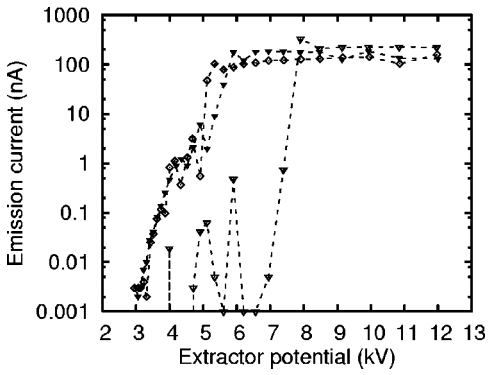

FIG. 23. Dark current *I-V* characteristics with onset of FEP (open triangles) where emission current starts much later than in subsequent *I-V* curves.

VI. DISCUSSION

The data shown here is generally consistent with the model given in section II. The shape of and changes in the *I-V* characteristics are well explained within this model, but it must be noted that they can also be explained in other models. The emission current in the plateau region depends on the concentration of free electrons in the depletion region, just as the dark current in a diode, which can be changed with temperature, intensity of light incident on the FEP and doping level (Figs. 8–10). The shape of the emitter tip has a large influence on the extraction voltage needed for emission, but this is generally true for field emitters (see different *I-V* curves Figs. 7, 8, 10, and 11). The stability of the emission current in regions 1, 3, and 4 is limited by the transparency of the surface vacuum barrier and therefore instable since residual gas atoms change the work function and shape constantly (Figs. 7 and 13). This effect is still visible in the instability of the angular current density in the plateau region (Fig. 15). Figure 11 clearly shows that the emission current is also related to the amount of surface defects. The largest component of the two mechanisms determines the height of the dark current plateau. The fact that passivation also has an effect on the light response (Fig. 11) shows that parts of the surface defects are located inside the depletion region. The current measured here is very stable (within 1% 3σ; see Fig. 12). However, we have shown in Fig. 16 that there are current bursts, which we associate with changes at the tip apex. We could only make them visible at extremely small cur-

rents, where the current increases instantaneously and decreases in about 500 ns to its original value, but we assume that they are also present at higher currents, where the peaks will be higher and shorter. It is found that the amount of electrons associated with this peak is typically about 600. The current peak is the result of the small capacitance of the emitter tip. Due to this capacitance (see Fig. 1) the current takes time to restore its original value. The finite response time after switching light intensities (Fig. 19) can also be assigned to the emitter tip capacitance. For large currents the charging of the capacitance takes less time than for small currents. Both in the largest current curve and the passivated curve in Fig. 20 a small overshoot is visible. This might be explained by a change in the size of the inversion layer when changing the intensity of the light incident on the FEP. With that, the capacitance also changes. This change results in a short excess of electrons which is however only temporary, so what results is a slow decay in current towards a new equilibrium situation. This is also clear from Fig. 20 where the capacitance is changed through the passivation of surface defects. The overall capacitance has become smaller and the change in capacitance by the light is now better visible in the overshoot in current. In Fig. 9 saturation of the emission current with increasing light intensity incident on the FEP is visible. This saturation is probably due to Auger recombination.[22] The excess carrier density becomes larger at higher light intensities, increasing the probability of an electron hole recombination, which results in the flattening of the curve. The current saturation at larger currents cannot be due to the fact that the surface vacuum barrier becomes the current limiting factor, because at 14 kV the data is extracted from the middle of the plateau region. The effect of Auger saturation is also visible in the plot of the quantum efficiency versus the light intensity (Fig. 22). The quantum efficiency drops clearly with increasing light intensity. The quantum efficiency measurements show that the quantum efficiency of *p*-type silicon can be over 100%. This is largely dependent on the resistivity where the lower resistivity here shows only a quantum efficiency of 10% (Fig. 22). For a smaller depletion region (smaller resistivity), the quantum efficiency is smaller because the generated electron-hole pairs are only separated inside the depletion region, in other words: The depletion region is the light sensitive area. The light sensitive area data (Fig. 21) shows the influence of both resistivity and light intensity on the size of the depletion layer. For larger resistivity (larger depletion region), the light sensitive area is clearly larger than for lower resistivity. The depletion region also increases with light intensity. The shift changes from the moment the diode becomes current limiting (Fig. 17). The fact that light incident on the FEP changes the diode is also the reason for the shift to change suddenly when the light intensity incident on the FEP changes. If the diode changes, the voltage drop over the diode also changes, resulting in an energy shift of the emitted electrons. An important result from these studies is the insight into the behavior of energy shift as a function of extraction voltage, emission current and light intensity. In combination with the occurrence of short current bursts, the energy shift behavior is the foundation of our conviction that the model of Sec. II is a good model for *p*-type semiconductor emitters.

A. Consequences for applications in lithography

The aim of the research on *p*-type silicon cold field emitters was the application in a lithography tool. In this section the consequences of our results for the application in lithography will be described. The emission current at illumination of the sample is more than sufficient. The dark current of the FEP can be limited sufficiently by employing a low resistivity and by reducing the amount of surface defects. Although the quantum efficiency decreases for a very low resistive FEP, the combination of an intermediate resistivity and surface passivation is shown applicable. The average stability of the emission current is within the requirement as well as the light response for large currents. The light response for typical currents used in lithography, however, is too slow but may be made within requirements with sufficient suppression of the amount of surface defects. The two main problems, which cannot be solved, are the instability of the apertured current and the energy shift instability. This energy instability results in a constant in-and-out of focus of the electron beam. Electron beams in lithography tools must be apertured in order to limit the aberrations of the lenses, particularly of the gun lens when the angle cannot yet be reduced. Another problematic effect of an unapertured beam is that there are current peaks consisting of about 600 electrons, which is a serious problem in lithography where per emitter only a few hundred electrons are used per pixel.

VII. CONCLUSIONS

We conclude that *p*-type silicon emitters are not suitable for application in a multibeam lithography tool. The research presented here, however, shows interesting physics and is, on most points, in agreement with a presented model for cold field emission from *p*-type semiconductors. The model consists of a mechanism of current stabilization by the energy shift. Measurements show clearly the stable emission current but unstable energy shift.

ACKNOWLDGMENTS

The authors wish to thank J. van der Does and P. P Crans for their outstanding technical support and fabrication of the measurement setups; DIMES and the TU Delft for support and the use of their facilities. This research was supported by the Dutch Technology Foundation STW.

[1]A. Aboubacar, A. Chbihi, and M. Querrou, J. Vac. Sci. Technol. B **13**, 616 (1995).
[2]A. Aboubacar, M. Dupont, and L. Says, Nucl. Instrum. Methods Phys. Res. A **13**, 74 (1994).
[3]R. Thomas and H. Nathanson, Appl. Phys. Lett. **21**, 387 (1972).
[4]P. P. Zavyalov, A. I. Klimin, and A. Yatsenko, Izv. Akad. Nauk SSSR, Ser. Fiz. **43**, 647 (1979).
[5]P. Kruit, J. Vac. Sci. Technol. B **16**, 3177 (1998).
[6]D. K. Schroder, R. N. Thomas, J. Vine, and H. C. Nathanson, IEEE Electron Device Lett. **21**, 785 (1974).
[7]L. Apker and E. Taft, Phys. Rev. **88**, 1037 (1952).

[8]J. Arthur, J. Appl. Phys. **36**, 3221 (1965).
[9]G. Busch and T. Fischer, Phys. Kondens. Mater. **1**, 367 (1963).
[10]R. Fischer and H. Neumann, Fortschr. Phys. **14**, 667 (1966).
[11]M. Baskin and G. Fursey, Phys. Status Solidi B **47**, 49 (1971).
[12]T. Hirano, S. Kanemaru, and J. Itoh, J. Vac. Sci. Technol. B **14**, 3357 (1996).
[13]D. Nicolaescu, J. Vac. Sci. Technol. B **11**, 392 (1993).
[14]R. N. Thomas, R. Wickstrom, D. Schroder, and H. Nathanson, Solid-State Electron. **17**, 155 (1974).
[15]R. Thomas and H. Nathanson, Appl. Phys. Lett. **21**, 384 (1972).
[16]Q. Huang, M. Qin, and J. Sin, J. Appl. Phys. **81**, 7589 (1997).
[17]R. Khatri, P. Asoka-Kumar, B. Nielsen, L. Roellig, and K. Lynn, Appl. Phys. Lett. **65**, 330 (1994).
[18]Y. Ha, S. Kim, S. Lee, J. Kim, D. Baek, H. Kim, and D. Moon, Appl. Phys. Lett. **74**, 3510 (1999).
[19]J. M. Bonard, J. P. Salvetat, T. Stockli, L. Forro, and A. Chatelain, Appl. Phys. A: Mater. Sci. Process. **69**, 245 (1999)
[20]G. N. Fursey *et al.*, Phys. Status Solidi **32**, 23 (1969).
[21]P. G. Borzyak *et al.*, Phys. Status Solidi **14**, 403 (1966).
[22]M. J. Kerr and A. Cuevas, J. Appl. Phys. **91**, 2473 (2002).